Observation of higher order radial modes in atomic layer deposition reinforced rolled-up microtube ring resonators

Jens Trommer,[1,2,3] Stefan Böttner,[1,*] Shilong Li,[1] Suwit Kiravittaya,[1,4] Matthew R. Jorgensen,[1] and Oliver G. Schmidt[1,5]

[1]*Institute for Integrative Nanosciences, IFW Dresden, 01069 Dresden, Germany*

[2]*Namlab gGmbH, Nöthnitzer Str. 64, 01187 Dresden, Germany*

[3]*Institut für Elektronik- und Sensormaterialien, TU Bergakademie Freiberg, 09599 Freiberg, Germany*

[4]*Department of Electrical and Computer Engineering, Faculty of Engineering, Naresuan University, Phitsanulok 65000, Thailand*

[5]*Material Systems for Nanoelectronics, Technische Universität Chemnitz, 09107 Chemnitz, Germany*

**Corresponding author: s.boettner@ifw-dresden.de*

Received July 25, 2014; revised September 30, 2014; accepted October 1, 2014; posted October 9, 2014 (Doc. ID 217377); published October 31, 2014

We present a detailed investigation of the resonator properties of high-quality rolled-up SiO_2 optical microtubes reinforced by atomic layer deposition. The evolution of the resonant modes with increasing film thickness and the transition to a multimode regime, including higher order radial modes, is discussed. Measurements and simulations show that the higher order modes exhibit high optical quality and an increased extension of the evanescent field from the resonator into the surrounding matrix, making them a promising solution for future on-chip sensor applications with increased sensitivity. © 2014 Optical Society of America

OCIS codes: (130.6010) Sensors; (230.3990) Micro-optical devices; (230.5750) Resonators; (250.5230) Photoluminescence; (310.1860) Deposition and fabrication.

http://dx.doi.org/10.1364/OL.39.006335

Vertically rolled-up microcavities (VRUMs) are a promising type of whispering-gallery-mode ring resonator [1–3]. As they are fabricated by a strain-induced roll-up process [4–6], they can be integrated on a large scale directly onto a microchip [6,7]. VRUM-based optical components such as add-drop filters [8], optical couplers [9], lasers [10] and optical sensor elements [11–15] have already been demonstrated.

Many applications require a mechanical reinforcement of the initial thin-walled tubular structure by atomic layer deposition (ALD) to increase their structural stability for postprocessing or operation. Concurrently, ALD coatings modify the spectral position of resonances and influence their quality-factor (Q-factor) [16–18]. Earlier, investigations focused on comparatively thin coatings and observed broad optical modes [16], which are inferior for sensing applications.

In this letter we show that this effect can be overcome using thicker coatings. We present a detailed investigation of the evolution of the resonator properties with increasing ALD layer thickness. We investigate the transition to a multimode regime where higher order radial modes are observed. These modes are identified and investigated by polarization and spatially resolved microphotoluminescence (μPL) mappings. In addition, we present results of numerical calculations showing that the evanescent fields from the higher order radial optical modes extend deeper into the surroundings, which is interesting for improving the sensitivity of on-chip optical sensors.

The VRUMs studied in this Letter are rolled-up from 70 nm-thick differentially strained patterned SiO_2 nanomembranes using well established fabrication techniques published elsewhere [3]. The resulting bridge-like VRUMs have an inner diameter of 15.3 μm and feature a wall thickness variation in the center leading to confinement of light in the axial direction [19]. Al_2O_3 was deposited in steps of 10 nm on the inner and outer wall of the VRUM leading to a 20 nm increase in tube wall thickness. Trimethylaluminium (TMA) and water were used as precursors at a substrate temperature of 200°C with 16 ms pulse time for both reactants. A long purge time of 10 s was used to ensure full desorption of the excess reactants inside the microtube. The VRUM shown in Fig. 1(a) is representative of VRUMs used in this study.

Optical characterization was performed on the same resonator after every ALD step using μPL. Excitation of the VRUMs at 442 nm leads to a broad emission band from 450 to 750 nm likely originating from defects [20] inside the SiO_2 layer. On top of this background, resonances appear as shown in Fig. 1(b). The resonant modes are formed by constructive interference of light traveling along the circumference of the tube and follow the simple approximation $\pi D n_{\text{eff}} = m\lambda$, where D is the

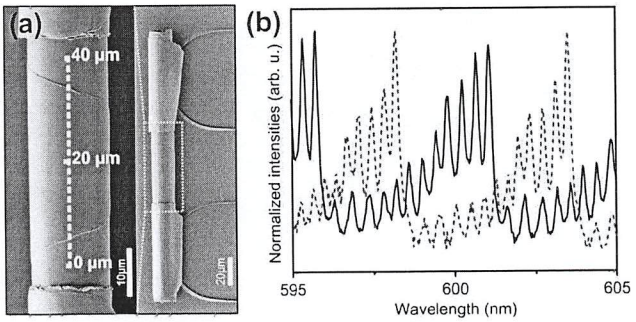

Fig. 1. (a) SEM images of a rolled-up microtube, focusing on the axial confinement facilitating lobe (left) and overall structure (right). The dashed line indicates the path followed for the mapping measurements displayed in Fig. 3(b). (b) Initial μPL emission signal of the VRUM showing three sets of azimuthal modes split up into axial modes (black line). The dashed red line shows a shift of the spectra due to desorption of water after heating for 10 min at 200°C in vacuum.

0146-9592/14/216335-04$15.00/0

VRUM diameter, n_{eff} the effective (group) refractive index, m the azimuthal mode number, and λ the wavelength of the resonant mode. The initial spectrum prior to ALD reveals three groups of azimuthal modes with mode numbers m from 107 to 109 within the spectral range of 592–608 nm that are formed due to the resonant properties of the VRUM. The mode numbers were estimated using numerical calculations using the model presented in [21]. Due to the thickness variation along the VRUM axis, an effective optical potential is created that leads to a splitting of each azimuthal mode m into narrow axial modes with Q-factors up to 3,300. The respective long wavelength peak in each azimuthal group is the axial mode of lowest order (see also as fabricated spectrum in Fig. 2). An additional similar splitting is, in principle, also possible due to the radial confinement of the VRUM wall leading to a split up into radial modes. However, without coating, only the lowest order (or fundamental) radial mode is confined, and only axial mode splitting is observed. Due to the symmetry of the VRUM, the modes also separate into a polarization state parallel (TM) and perpendicular (TE) respective to the VRUM axis. For thin-walled VRUMs, only TM polarized light is supported, while out of plane TE polarized modes are less confined, as their electric field is not continuous at the wall–air interface and therefore subject to higher losses [22].

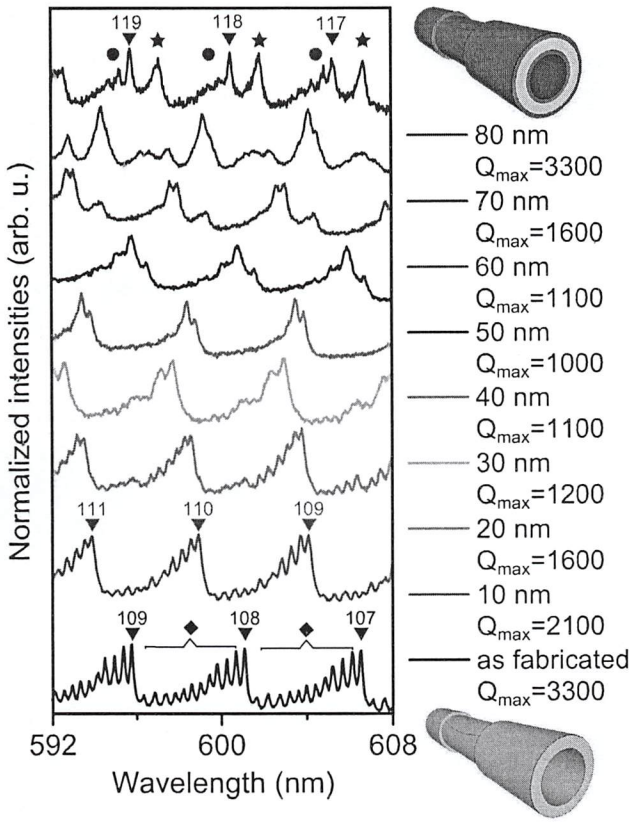

Fig. 2. Evolution of the μPL emission signal of the rolled-up microcavity shown in Fig. 1 as a function of ALD single-layer thickness. TM polarized azimuthal modes split up into a set of higher order axial modes (diamonds) and corresponding lowest order axial modes (triangles) are marked in the initial spectrum with respective azimuthal mode number m. In the spectrum from the most thickly coated resonator TM_0 (triangles) and TM_1 (stars) radial modes as well as TE polarized modes (circles) are visible. As they do not necessarily belong to the same azimuthal mode number, values for m are indicated only for TM_0. Q_{max} denotes the highest measured quality-factor for each mode spectrum. Tube schematics show an uncoated and coated resonator, respectively.

Prior to the ALD deposition, the VRUMs were kept in the ALD chamber under vacuum for 2 h at 200°C to ensure that their optical quality is not degraded by the process conditions of the machine (Savannah 100, Cambridge Nanotech). Spectra taken before and after this heating procedure are shown in Fig. 1(b). The VRUM maintains its sharp resonances, and also all 12 resonances per group are unaffected. Only the absolute mode positions of the whole spectrum are shifted by ~3 nm, which can be attributed to a desorption of water from the resonator surface [14,17].

When the tube is coated with ALD, the effective refractive index and the wall thickness are gradually changed leading to the predicted continuous redshift [16] of the modes in the μPL spectra shown in Fig. 2. Note that the redshift induced with every step is very large as can be seen by the first two spectra. In addition, we observed that the axial modes started to overlap with increasing coating thickness, while the number of observed axial modes decreased. At an Al_2O_3 layer thicknesses of 30–40 nm, no clear identification of axial modes is possible anymore as shown in the μPL spectrum in Fig. 2. This is likely due to the decreased significance of the lobe engineered into the rolled-up structure, which accounts for an increased average wall thickness of 47% in the uncoated tube but only 27% when there is a 40 nm thick coating. The optical axial potential well correspondingly decreases as the walls become uniformly thicker, an effect which also explains the decrease in Q_{max} as reported in [23]. However, when the coating process is continued, the radial confinement is enhanced and the tube gradually reaches the multimode regime where higher order radial TM modes and perpendicular polarized TE modes can be confined. This can be nicely seen in Fig. 2, while the coating thickness increases from 30 to 80 nm, the spectra start to include first broad modes and then additional narrow peaks. We will later identify the broad modes as TE_0 and the narrow peaks as higher order radial TM_1 modes.

Since the electric field distribution of each type of mode is different, their unequal sensitivity to the coating leads to the peaks shifting by different magnitudes, including the case of spectrally overlapping mode peaks. At 40 nm, it is for example difficult to find a TE mode. This is crucial from an application point of view, as many enhancement layers reported so far focused on mechanical stabilization with coatings in a narrow range from 30 to 60 nm [12–14,16], and were not optimized with respect to clearly separated modes in the desired spectral range. Thus, we continued coating until a sufficient separation of the modes was achieved at an ALD thickness of 80 nm, which simplifies a detailed investigation. Of particular interest at this point are the two sharp intense peaks that have high Q-factors (3300 and 2200) compared to the intermediate spectra. We attribute the high Q to the increase in radial confinement during the coating process, leading to an n_{eff} of 1.58 after 80 nm of Al_2O_3 coating

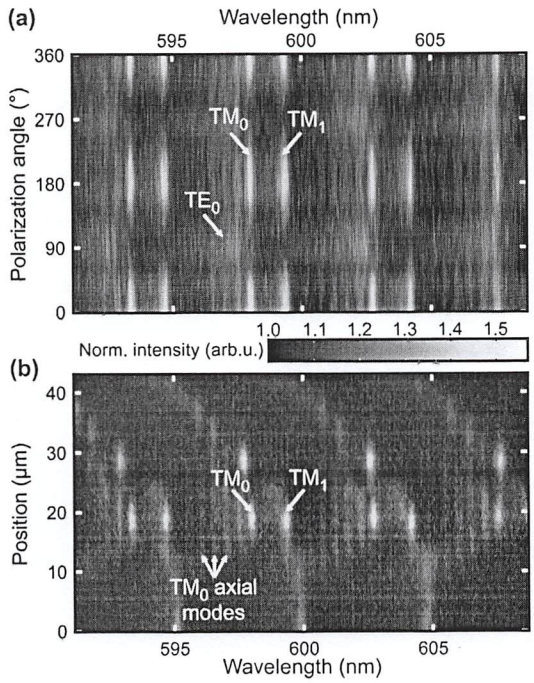

Fig. 3. (a) Polarization mapping and (b) spatial mapping of VRUM coated with 80 nm Al_2O_3. TM_0, TM_1 and TE_0 peaks are identified as described in the text. The azimuthal order of the TM_1 modes is presumably different from TM_0.

compared to 1.41 for the uncoated resonator. This effect overcompensates the quality loss due to the decreased axial confinement, which has not been observed for thin ALD coatings [16].

From the μPL spectra it is difficult to distinguish between TM and TE modes, axial modes and higher order radial modes. To experimentally identify the different TM and TE modes, a map of the μPL as a function of the polarization angle, as shown in Fig. 3(a), was performed. For each set of modes, two sharp peaks are observed at 0° and 180° corresponding to TM polarized modes. Very broad peaks, corresponding to TE polarized modes, are observed at orthogonal polarization at 90° and 270°.

In order to distinguish the two TM modes, the mode signature of the VRUM was additionally explored by a spatially resolved PL mapping along the tube axis at a polarization angle of 180°, to clearly reveal and identify possible axial modes, as shown in Fig. 3(b). The two sharp TM polarized modes were observed at the center of the lobe area of the tube [around 20 μm away from the starting scanning position, see Fig. 1(a)]. Weak axially split modes with their characteristic spatial distribution along the axis are apparent in the map at shorter wavelengths that were not clearly visible in the spectra in Fig. 2. The asymmetric spatial distribution, with respect to the center position, can be attributed to an increasing VRUM diameter along the axis due to an asymmetric roll-up as discussed in detail previously [24]. The free spectral range of the axial modes is narrow compared to the spacing of the peaks labeled with TM_0 and TM_1, which suggests that the TM_1 labeled peak is not merely another TM_0 axial mode but genuinely a higher order radial mode. This conclusion is also supported by the different shift during coating.

Moreover another high-quality TM mode can be found at an off-centered position of 30 μm, which does not seem to belong to axial modes. We attribute this to a second optical confinement at this position due to the slight asymmetric rolling process and possible corrugations that lead to spatially pinned resonances as reported in [25]. Because this peak only appears when directly excited in the near field, it is not visible in the spectra in Fig. 2.

To compare the sensing properties of coated and uncoated tubes, we calculated the electric field distribution of the different mode types within our resonator using the Helmholtz wave equation for ring structures with parameters measured from our real tube. First, it can be seen in Fig. 4 that the evanescent field of the TM_0 mode decreases with increased ALD coating, due to an increased confinement. In contrast, the TE_0 and TM_1 modes show a larger evanescent field in the hollow core of the resonator, which is associated with a high sensitivity [26,27]. Indeed, the TM_1 mode shows the largest extension of the evanescent field in the hollow core of

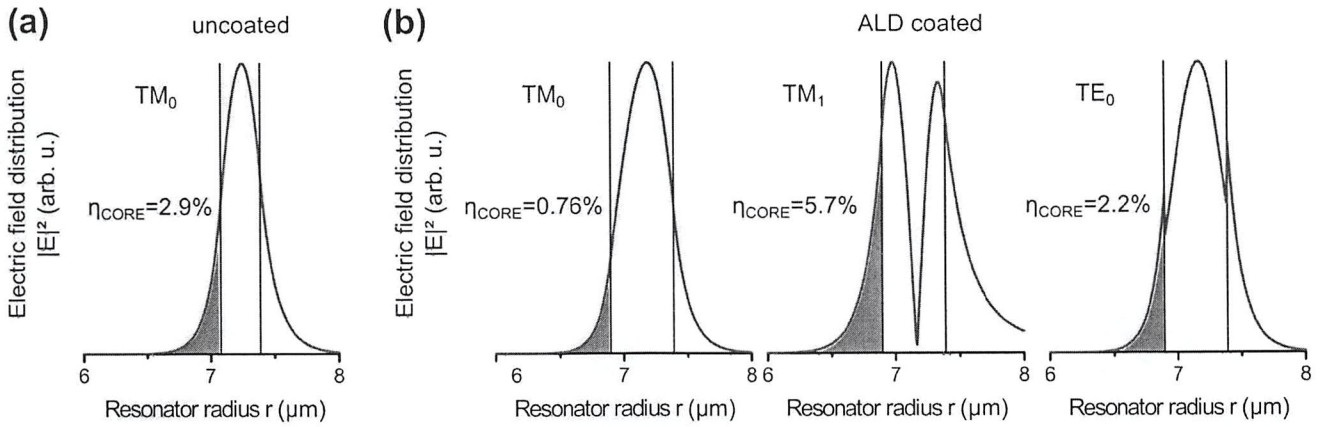

Fig. 4. Electric field distribution of TM_0, TM_1 and TE_0 modes in the (a) uncoated and (b) coated resonator, as a result of waveguide simulations using parameters of our measured VRUM. The energy fraction in the hollow core η_{CORE} is given and marked in blue. The calculations show that the evanescent field of the TM_1 modes extends more into the hollow core of the tubular resonator than for other modes, which is a direct indicator of the optical sensitivity [26,27].

the tube with an energy fraction of 5.7%: nearly double that of the TM_0 mode of the uncoated tube. In addition, the Q-factor of our identified TM_1 mode is distinctly higher (2,200) compared to TE_0, as they do not suffer from discontinuities in the field distribution at the resonator surface [22], making tubular resonators with higher order radial TM_1 modes a promising alternative for on-chip sensing applications.

To summarize, we have investigated the influence of a conformal ALD reinforcement layer on the resonator properties of a tubular vertically rolled-up microcavity. We have shown that a thin coating is inadequate for sensing applications, due to a loss of axial confinement and broadening of the peaks. However, we found that the resonator shifts into a radial multimode regime with clearly distinguishable single and higher order TM modes with reasonable quality factors of up to 3,300 with continued coating. Calculations show that especially the TM_1 mode is promising for sensing applications, as it exhibits a higher fraction of evanescent field extending into the hollow core of the tubular resonator, leading to an increased sensitivity.

We greatly appreciate technical support from S. Harazim, R. Engelhard and D. Grimm. This work was supported by the Volkswagen Foundation (I/84072), and the DFG priority program FOR 1713. S. L. Li thanks the financial support from China Scholarship Council (CSC, File No. 2008617109).

References

1. R. Songmuang, A. Rastelli, S. Mendach, and O. G. Schmidt, Appl. Phys. Lett. **90**, 091905 (2007).
2. T. Kipp, H. Welsch, Ch. Strelow, Ch. Heyn, and D. Heitmann, Phys. Rev. Lett. **96**, 077403 (2006).
3. S. Böttner, S. L. Li, J. Tronmer, S. Kiravittaya, and O. G. Schmidt, Opt. Lett. **37**, 5136 (2012).
4. V. Y. Prinz, V. A. Seleznev, A. K. Gutakovsky, A. V. Chehovskiy, V. V. Preobrazhenskii, M. A. Putyato, and T. A. Gavrilova, Phys. E Low-Dimens. Syst. Nanostructures **6**, 828 (2000).
5. O. G. Schmidt and K. Eberl, Nature **410**, 168 (2001).
6. Y. F. Mei, G. S. Huang, A. A. Solovev, E. B. Ureña, I. Mönch, F. Ding, T. Reindl, R. K. Y. Fu, P. K. Chu, and O. G. Schmidt, Adv. Mater. **20**, 4085 (2008).
7. S. M. Harazim, W. Xi, C. K. Schmidt, S. Sanchez, and O. G. Schmidt, J. Mater. Chem. **22**, 2878 (2012).
8. S. Böttner, S. L. Li, M. R. Jorgensen, and O. G. Schmidt, Appl. Phys. Lett. **102**, 251119 (2013).
9. S. Bhowmick, J. Heo, and P. Bhattacharya, Appl. Phys. Lett. **101**, 171111 (2012).
10. F. Li and Z. Mi, Opt. Express **17**, 19933 (2009).
11. A. Bernardi, S. Kiravittaya, A. Rastelli, R. Songmuang, D. J. Thurmer, M. Benyoucef, and O. G. Schmidt, Appl. Phys. Lett. **93**, 094106 (2008).
12. S. M. Harazim, V. A. Bolaños Quiñones, S. Kiravittaya, S. Sanchez, and O. G. Schmidt, Lab Chip **12**, 2649 (2012).
13. G. S. Huang, V. A. Bolaños Quiñones, F. Ding, S. Kiravittaya, Y. Mei, and O. G. Schmidt, ACS Nano **4**, 3123 (2010).
14. L. Ma, S. Li, V. A. Bolaños Quiñones, L. Yang, W. Xi, M. Jorgensen, S. Baunack, Y. Mei, S. Kiravittaya, and O. G. Schmidt, Adv. Mater. **25**, 2357 (2013).
15. E. J. Smith, S. Schulze, S. Kiravittaya, Y. Mei, S. Sanchez, and O. G. Schmidt, Nano Lett. **11**, 4037 (2011).
16. V. A. Bolaños Quiñones, G. S. Huang, J. D. Plumhof, S. Kiravittaya, A. Rastelli, Y. Mei, and O. G. Schmidt, Opt. Lett. **34**, 2345 (2009).
17. J. Zhong, J. Wang, G. S. Huang, G. Yuan, and Y. Mei, Nanoscale Res. Lett. **8**, 1 (2013).
18. J. Wang, G. S. Huang, and Y. Mei, Chem Vap. Deposion **20**, 103 (2014).
19. Ch. Strelow, H. Rehberg, C. M. Schultz, H. Welsch, Ch. Heyn, D. Heitmann, and T. Kipp, Phys. Rev. Lett. **101**, 127403 (2008).
20. L. B. Ma, T. Schmidt, C. Jäger, and F. Huisken, Phys. Rev. B **82**, 165411 (2010).
21. S. L. Li, L. B. Ma, S. Böttner, Y. F. Mei, M. R. Jorgensen, S. Kiravittaya, and O. G. Schmidt, Phys. Rev. A **88**, 033833 (2013).
22. Ch. Strelow, C. M. Schultz, H. Rehberg, M. Sauer, H. Welsch, A. Stemmann, Ch. Heyn, D. Heitmann, and T. Kipp, Phys. Rev. B **85**, 155329 (2012).
23. M. Sumetsky, Opt. Lett. **35**, 2385 (2010).
24. V. A. Bolaños Quiñones, L. B. Ma, S. L. Li, M. R. Jorgensen, S. Kiravittaya, and O. G. Schmidt, Opt. Lett. **37**, 4284 (2012).
25. Ch. Strelow, C. M. Schultz, H. Rehberg, H. Welsch, Ch. Heyn, D. Heitmann, and T. Kipp, Phys. Rev. B **76**, 045303 (2007).
26. H. Zhu, I. M. White, J. D. Suter, P. S. Dale, and X. Fan, Opt. Express **15**, 9139 (2007).
27. J. Zhang, J. Zhong, Y. Fang, J. Wang, G. Huang, X. Cui, and Y. F. Mei, Nanoscale **6**, 13646 (2014).

สำเนาถูกต้อง

Sunit Kiravittaya